

Enhanced Fatigue Life in GFRP Composites: A Comparative Study of Wet Lay-up vs. Vacuum Assisted Resin Transfer Molding for Small-Scale Wind Turbine Blades

Mehran Toghraee¹, Ahad Zabett^{1*}, Sirius Javadpour², Pouya Valizadeh¹

¹ Ferdowsi University of Mashhad, Iran, Sun Air Research Institute, Department of Materials Science and Engineering, Mashhad, 9177948944

² Shiraz University, Iran, Department of Materials Science and Engineering, Shiraz, 8433471946

Abstract:

Wet lay-up and vacuum-assisted resin transfer molding have been conceived as the most popular and cost-effective manufacturing processes of E-glass fiber reinforced epoxy-based laminated composite, especially in the wind turbine blade manufacturing industry. This study compares the fatigue behavior of GFRP laminated composites manufactured via wet lay-up and vacuum-assisted resin transfer molding processes. Vacuum-assisted resin transfer molding samples exhibited 85% longer fatigue life at a stress level of 0.4 ultimate tensile strength compared to wet lay-up samples. The average ultimate tensile strength of vacuum-assisted resin transfer molding samples was 50% higher, with improved fatigue resistance due to enhanced fiber-matrix bonding. Scanning electron microscopy fracture analysis revealed improved fiber/matrix bonding in vacuum-assisted resin transfer molding fatigued samples, contributing to enhanced fatigue performance. These findings provide critical insights for wind turbine blade material selection and optimization. The results indicate that vacuum-assisted resin transfer molding composites sustain 4.5 more load cycles at lower stress levels, demonstrating superior fatigue performance for wind turbine blades.

Keywords:

Vacuum-assisted Resin Transfer Molding, Wet Lay-up, Fatigue properties, E-glass Fiber Reinforced Epoxy laminated composites, Fatigue failure mechanism, Wind turbine blade

* Corresponding author, Email: ahad@um.ac.ir

1 Introduction

The manufacturing of wind turbine blades relies on various techniques, with Wet Lay-up (WL) and Vacuum Assisted Resin Transfer Molding (VARTM) being among the most prominent. Hsiao et al. (1) describe WL as a traditional and well-known small and medium-scale wind turbine blade manufacturing process. This process involves placing layers of dry fibers into an open mold, followed by the manual application of liquid resin, which is then impregnated into the fibers using tools like rollers or brushes to ensure complete wetting and uniform distribution of the resin. Although WL offers simplicity, lower tooling costs, and flexibility in accommodating complex shapes (2), it is labor-intensive and can result in manufacturing defects such as air bubbles, dry spots, and inconsistent fiber volume fractions, leading to composites with less uniform mechanical properties. Olabi et al. (3) emphasized that these defects significantly reduce fatigue resistance, making WL less suitable for long-term structural applications.

In contrast, VARTM has become the preferred method for producing large-scale, geometrically complex glass fiber-reinforced polymer (GFRP) laminated structures, including wind turbine blades (4). In VARTM, dry fibers are placed in a mold and covered with a resin flow medium and plastic bag. The system is then sealed and subjected to negative pressure, which facilitates the thorough impregnation of fibers with resin while the excess resin is evacuated from the mold (5), resulting in a composite with a higher fiber volume fraction (6) and fewer defects. This process not only enhances the structural integrity and durability of the resulting blades but also allows for better control over resin distribution (7), which is critical for maintaining mechanical properties under operational conditions. Studies by Lusty et al. (8) have shown that VARTM enhances fatigue life by increasing fiber volume fractions and improving fiber-to-resin ratios compared to hand lay-up methods. From a sustainability perspective, VARTM offers reduced material waste due to controlled resin flow and vacuum infusion, leading to higher efficiency and lower emissions (9). Conversely, WL results in higher resin wastage, increased VOC emissions, and inconsistent fiber distribution, contributing to material inefficiencies.

GFRP laminated composites are widely favored in load-bearing components, particularly in applications where a high stiffness-to-density ratio is essential (10). Despite their advantages, the replacement of traditional materials like metals with GFRP composites is limited by the variability in their physical and mechanical properties, which can significantly influence fatigue performance. Fatigue is a leading cause of failure in in-service structures (11), making it crucial to predict the service life of GFRP composites under cyclic loading. The fatigue life of GFRP composites is influenced by factors such as constituent properties, fiber volume, ply termination, moisture, and the manufacturing process (12-16). Research has demonstrated that the higher fiber volume fractions achieved through VARTM significantly enhance mechanical properties by increasing stiffness, minimizing resin-rich regions, and improving load transfer efficiency between fibers. These factors collectively contribute to greater resistance to cyclic loading, leading to composites with extended service life and improved durability under fatigue conditions (17). Unlike metals, GFRP composites exhibit complex fatigue behavior due to the interplay of these factors, requiring re-evaluation during the

design phase (18). Fatigue stress exposure in composite structures is evaluated using sector-based load representation, where the damage calculation depends on the negative inverse slope of the S-N curve, ensuring accurate fatigue life predictions (19).

Wind turbine rotor blades, predominantly made of GFRP composites, experience significant fatigue loading (up to 10^8 to 10^9 load cycles over a 20-year lifespan), which is influenced by nominal power settings, wind speed fluctuations, and operational conditions (20). Existing studies on the fatigue behavior of GFRP composites in wind turbine applications have primarily focused on alternative reinforcements and numerical modeling rather than direct manufacturing method comparisons. Kim & Cho (21) explored graphene-reinforced composites for fatigue life enhancement using numerical analysis but lacked direct experimental validation under real fatigue conditions. Similarly, Zheng et al. (22) examined basalt fiber-reinforced composites for offshore applications but did not compare them to traditional GFRP wind turbine materials. Pathak et al. (23) investigated recycled glass-epoxy composites, prioritizing sustainability rather than direct fatigue performance comparison between manufacturing methods. Despite these advances, uncertainties remain in predicting the long-term reliability of these composites under cyclic loading (24). Moreover, while studies acknowledge the superior fatigue resistance of VARTM-manufactured composites, direct comparative analyses of the fatigue performance of blades manufactured using WL and VARTM under identical conditions are limited. This study addresses this gap by providing an experimental comparison of VARTM and WL-manufactured GFRP composites, focusing on fatigue life, failure mechanisms through SEM imaging, and Weibull reliability assessments under controlled fatigue loading conditions. By integrating these insights, this research contributes to optimizing manufacturing selection for small and medium-scale wind turbine blade applications, ensuring improved fatigue durability and reliability in operational environments.

Experimental Procedure

The E-glass fiber-reinforced polymer (GFRP) laminated composite sheets of $500 \times 500 \times 2$ mm³ were fabricated using two different manufacturing processes: VARTM and WL. In the VARTM process, a vacuum pump was used to maintain the pressure at about 0.9 bar. The resin infusion rate was measured at approximately 0.28 mL/S, corresponding to a total infusion time of 140 minutes for complete saturation of the fiber pre-form. During fabrication, fiber fabrics, peel ply, and resin flow were precisely cut and placed on the mold coated with separator-coating wax. The layers were fixed using FusionFix™ GP adhesive spray to ensure the correct stacking sequence and fiber orientation. The vacuum setup, including the resin infusion spiral, vacuum hoses, inlet, outlet, valves, and sealant tapes, was properly implemented and tested for leaks before initiating the infusion process. The laminates were cured at 23 °C and 40% RH for 24 hours and post-cured at 75°C for 16 hours. To ensure consistency in physical and mechanical testing, test coupons were cut out from the fabricated laminates using a water jet cutting technique. Samples were cut along the 0° fiber direction, aligning with the principal load-bearing orientation.

All sheets and specimens were fabricated under industrial conditions representative of the actual manufacturing setup used in the production of small and medium-sized wind turbine blades. This ensured that the material processing, environmental parameters, and quality control measures reflect those encountered in full-scale industrial blade fabrication, thereby enhancing the practical relevance and applicability of the results.

- Materials and Fabrication

The GFRP composite laminates were constructed using unidirectional and cross-ply E-glass stitched fabrics (STA 090/300-8208000), featuring area densities of 165 g/m² for 0° fibers and 130 g/m² for 90° fibers. A low-viscosity epoxy resin was used to impregnate the fabrics for both manufacturing processes. Axson technologies EPOWIND® EPOLAM 2040 epoxy resin, mixed with EPOLAM 2047 hardener in a 100:32 weight ratio, served as the polymer matrix. Table 1 summarizes the tensile and physical properties of the GFRP composite constituents used in this study.

The stacking sequence of the laminates was designed to replicate the lay-up used for a 100 kW wind turbine blade (SARI 100 kW) at the Sun Air Research Institute (SARI). The [90/0/±45/0]_{ns} lay-up was chosen as it represents a repeating structural unit within the actual turbine blade, ensuring that the test specimens closely reflect real-world applications.

Table 1 - Tensile and physical properties of the used GFRP composite constituents.

Material	Description	Density (g/cm ³)	Ultimate Tensile Strength (MPa)	Elastic Modulus (GPa)
Fiber	E-Glass stitched fabrics (STA 090/300-8208000) at 0 °	2.55	3450	72
Resin	EPOLAM 2040 at 25 C°	1.16	75	3.5
Hardener	EPOLAM 2047 at 25 C°	0.94	71	3.5

- Sample Fabrication

The test specimens were carefully cut out from the fabricated sheets to ensure uniformity in fiber orientation and minimize variability in mechanical properties. The cutting direction was maintained parallel to the primary load-bearing 0° fiber direction, ensuring that fatigue and tensile tests accurately represented in-service conditions. Figure 1 illustrates the fiber architecture and sample extraction process, providing a clear visualization of the specimen preparation methodology.

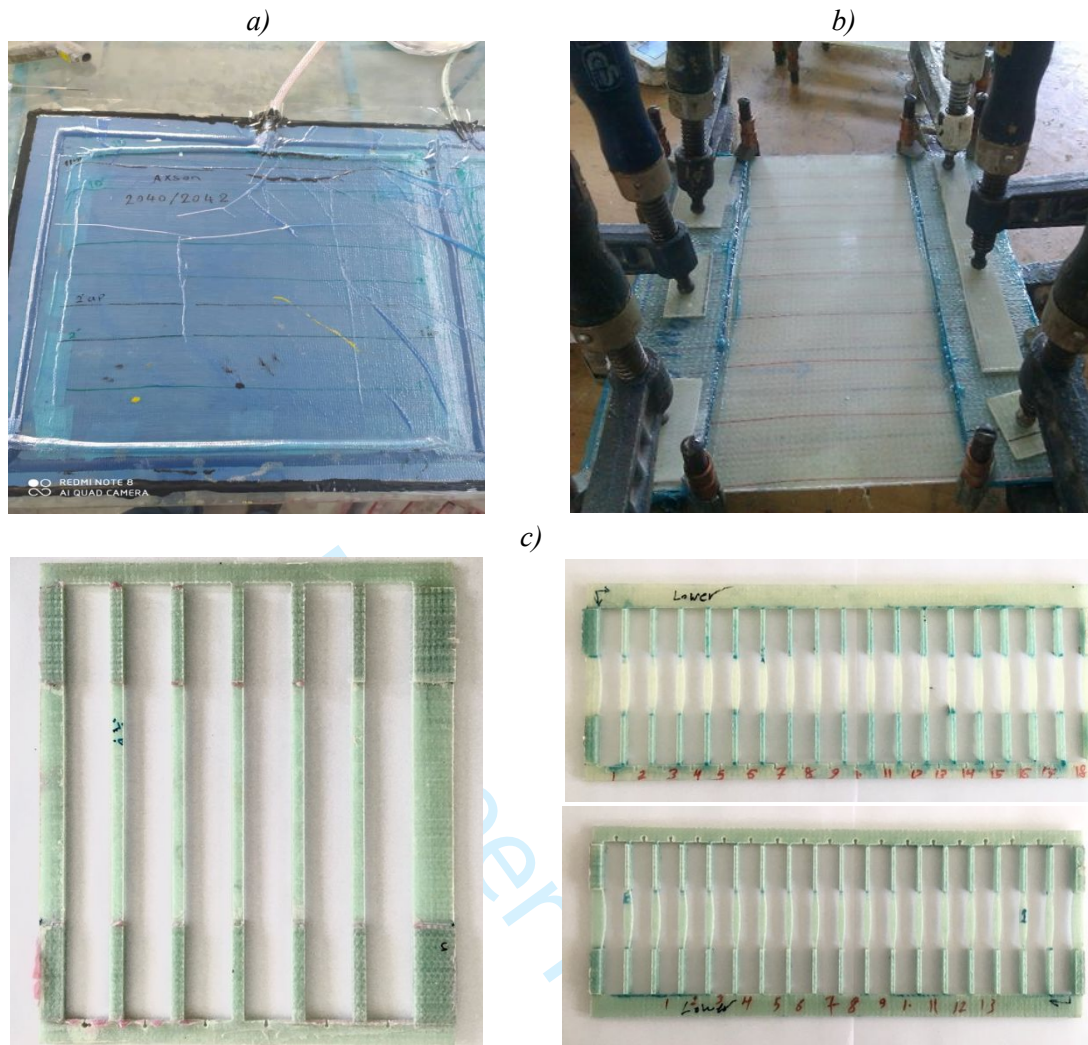


Figure 1- Sample fabrication stages a) sheet fabrication (VARTM set-up) b) bonding tabs c) cutting out test specimens from the sheets

- Characterization method

The fabricated samples were physically and mechanically (static and dynamic) tested with reference to the DNV GL guideline (25) as follows:

Burn-off test: To determine the void and fiber volume content of manufactured sheets, a set of six samples for each series of manufactured GFRP was prepared and tested according to the ASTM D2734 standard (26). The weight and density of samples were measured using analytical balance Precisa XB 120A with a capacity of 120 g, while the samples were heated at 560 °C for 5 hours. Figure 2a (26) shows the burn-off coupon geometry.

Tensile test: Tensile properties of the laminated GFRPs were measured based on the ASTM D3039 standard (27). Zwick Z250 universal testing machine was used, under displacement control until fracture at a crosshead speed of 2 mm/min and ambient temperature. Force was measured directly by the load cell of the Zwick Z250 machine, which has an accuracy of $\pm 0.5\%$. Strain was recorded using a clip-on axial extensometer with a gauge length of 50 mm, which has an accuracy of $\pm 2 \mu\text{m}$. The GFRP laminate was bonded with an adhesive

epoxy film as end tabs to minimize the risk of tab failure during tensile tests. To minimize the risk of premature failure, all samples were clamped carefully onto the wedge jaws and checked dimensionally at the grip to prevent any potential misalignment before testing. Figure 2b (27), demonstrates the tensile coupon geometry. A total of 15 tensile samples were tested (six samples for WL and nine samples for VARTM). This number of samples complies with minimum data requirements for statistical confidence, as suggested in ASTM D3039 standard (27), ensuring the robustness of the comparison.

Fatigue test: A total of 59 specimens were subjected to constant amplitude (CA) fatigue loading using a servo-hydraulic universal fatigue testing machine with a 25 kN load capacity. This number of samples complies with the minimum data requirements for statistical confidence, as suggested in DNVGL-ST-0376 (25). The tests were conducted under force-controlled conditions with a sinusoidal tension-tension waveform at room temperature. Samples were clamped using a screw-fitting fixture. A stress ratio (R) of 0.1, as recommended by DNVGL-ST-0376 (25), was employed to replicate operational fatigue loading conditions in wind turbine blades. This ratio is widely utilized for assessing fatigue damage in laminated composites under cyclic tension loading (28-30). The test frequency was set at 8 Hz, balancing efficient test duration while limiting heat buildup to below 35°C (31). Although higher frequencies are theoretically feasible for stiff composite materials, this frequency was selected to prevent excessive self-heating, which could modify fatigue failure mechanisms and compromise result accuracy. This selection was based on complementary project studies investigating the stress-dependent creep behavior of Glass/Epoxy composites on similar GFRP samples (32 and 33). The fatigue tests were designed to generate a full S-N curve, targeting cycle ranges between 10^4 and 10^6 cycles to evaluate both high-cycle fatigue behavior and progressive damage accumulation.

To ensure consistency and reliability, dog-bone-shaped specimens were used to enhance repeatability and mitigate grip failures. The specimen edges were meticulously polished with silicon carbide paper (up to 1200 grit) to remove microcracks induced by water jet cutting, following ASTM D3479-96 guidelines (34). Additionally, adhesive epoxy end tabs were affixed to the specimens to minimize stress concentrations at the grips. Specimens were secured using screw clamps, ensuring stable placement, uniform load distribution, and preventing slippage during cyclic loading.

Fatigue tests were conducted at four stress levels, ranging from 0.2 to 0.6 of the ultimate tensile strength, in accordance with DNVGL-ST-0376 test design recommendations (25). To avoid premature failure, specimens were gradually loaded to their minimum and maximum stress levels over approximately 600 cycles, ensuring uniform stress distribution throughout testing. Coupon surface temperature was continuously monitored using a thermometer, with a strict 35°C threshold to prevent thermal degradation of the polymer matrix. Figure 2c (34) illustrates the flat dog-bone specimen geometry, adapted from Dyer's (35), Mandell's (36) and Valizadeh et al. (24). To ensure statistical robustness, at least six valid data points (failures occurring within the gauge length) were recorded at each stress level.









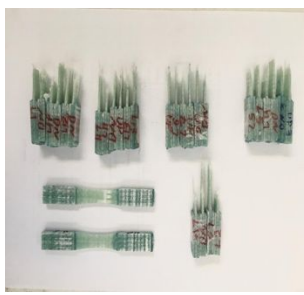
Scanning Electron Microscopy (SEM) analysis: Aiming at a comprehensive comparison between these two types of samples, the fracture surfaces of each series were investigated using

the SEM. To ensure comparability, samples were selected from various stress levels (0.2–0.6 of UTS) and corresponding cycle numbers, enabling a consistent comparative analysis of failure mechanisms between the two manufacturing methods. To enhance imaging clarity and identify the dominant fatigue failure mechanisms, the fracture surfaces were sputter-coated with a thin layer of gold before analysis. SEM imaging was performed using a LEO-1450VP scanning electron microscope, operated at an accelerated voltage of 20 kV.

Thermogravimetric analysis (TGA) analysis: TGA was performed separately on pure resin, fiber, and two types of GFRP composites (manufactured using VARTM and WL processes) to determine the resin-to-fiber weight ratio and compare the thermal resistance of the composites. The analysis was carried out using a BAHR STA 503 instrument, following ASTM E113 (37), under an argon flow rate of 10 ml/min, up to a maximum temperature of 900 °C.

Images of the fabricated samples before, during, and after fatigue testing, illustrating the setup and damage evolution, were shown Table 2.

Table 2 - Photographic documentation of tested samples at different stages of fatigue testing.

Test	Before Test	During Test	After Test
Burn-off			
Tensile			
Fatigue			

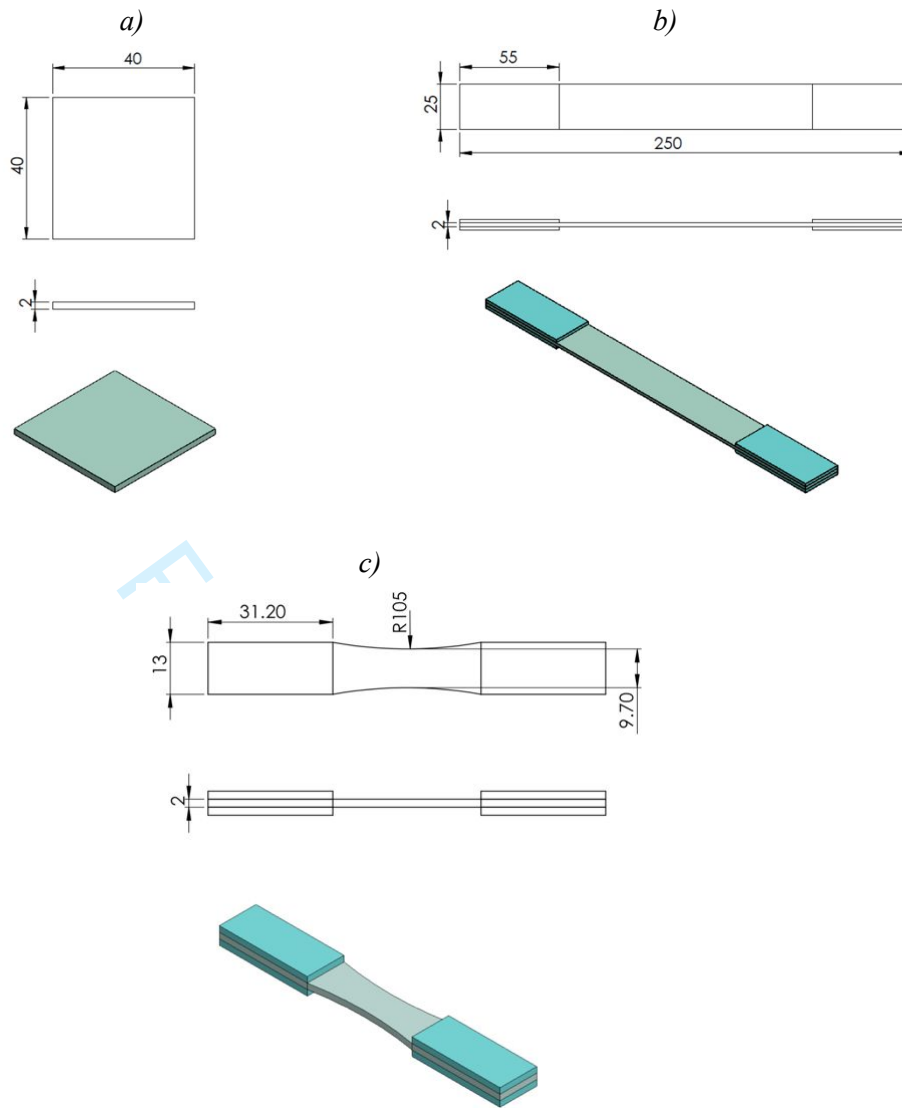


Figure 2- Specimen geometry for a) Burn-off (26) b) Tensile (27) and c) Fatigue (34) in mm.

Results and Discussion

The average fiber weight percentages for the WL and the VARTM-manufactured GFRPs were 52 % (standard deviation (SD) 4.36, coefficient of variation (CV) 0.084) and 69 % (SD 0.89, CV 0.013), respectively. This notable difference in fiber content significantly enhanced the mechanical properties of VARTM samples compared to WL samples. The measured weight percentages were consistent with TGA records, indicating thermal resistance parity between both manufacturing processes at the initial degradation temperature (340 °C). This temperature is slightly higher than that of the pure resin, with a weight retention of 98%. The slight difference between the GFRPs and the pure resin suggests that the fiber surface treatment was insufficient to improve mechanical cross-linking among the GFRP constituents (38).

Due to the inhomogeneous and anisotropic nature of composite materials and the stochastic characteristics of the fatigue process, experimental results exhibited significant variability even under controlled testing conditions. To assess the reliability of composite structures, the

distribution uniformity of tensile strength and fatigue results was analyzed using a two-parameter Weibull distribution based on Bedi's methodology (39).

Tensile properties were evaluated to establish fatigue test loads and compare the tensile properties of the two manufacturing processes. The results, summarized in Table 3, include the Weibull shape (α) and scale (β) parameters as well as the average ultimate tensile strength (σ_{ut}) and average ultimate tensile strain (A_t).

Table 3 shows that the σ_{ut} of VARTM samples is 50% higher than that of WL samples, while the difference in A_t is approximately 4%. The higher α value (40) of the VARTM samples further indicates more consistent tensile performance compared to WL samples. This enhanced reliability is primarily attributed to the vacuum pressure applied during the VARTM process, which significantly reduces manufacturing defects such as voids, resin-rich regions, and fiber misalignment. Additionally, the process improves matrix-fiber interfacial bonding, as confirmed by SEM analysis.

Table 3- Tensile properties of the WL and VARTM manufactured GFRPs.

Manufacturing Process	Sample Size (pcs)	Ultimate tensile Strain (%)			Ultimate Tensile Strength - UTS (MPa)				
		A_t	SD	CV	σ_{ut}	SD	CV	Weibull shape parameter (α)	Weibull scale parameter (β)
WL	6	2.21	0.164	0.074	249.2	12.46	0.05	17.89	256
VARTM	9	2.31	0.162	0.073	374.9	15.74	0.042	18.91	385.3

Fatigue data was converted to $R = -1$ using the Goodman relation (41), allowing direct comparison with established fatigue models and ensuring consistency with literature results, as per Eq. 1.

$$\sigma_{fat} = \frac{\sigma_a}{1 - \frac{\sigma_m}{\sigma_{ut}}} \quad \text{Eq. 1}$$

Where σ_a is the alternating stress, σ_m is the mean stress, and σ_{ut} is the ultimate tensile strength. σ_{fat} represents the equivalent stress amplitude in the fully reversible state. By substituting $\sigma_a = 0.45\sigma_{max}$ and $\sigma_m = 0.55\sigma_{max}$ ($R=0.1$), Eq. 1 can be rearranged as:

$$\sigma_{max} = \frac{\sigma_{fat}}{45 - \frac{55\sigma_{fat}}{\sigma_{ut}}} \quad \text{Eq. 2}$$

Using the σ_{ut} value obtained from tensile test for each manufacturing process, the σ_a and its corresponding forces (F_{min} and F_{max}) can be determined using Eq. 2. Since both σ_{ut} and σ_{fat}

are known, σ_a and the associated forces, F_{min} and F_{max} , can be calculated from the same equation.

Fatigue test results at four stress levels were fitted using the two-parameter Weibull distribution, with α and β representing the shape parameter and characteristic life (scale parameter) at the proposed σ_{fat} , respectively. Detailed fatigue results are presented in Table 4.

Table 4- Fatigue tests results of the WL and VARTM manufactured GFRPs.

Manufacturing Process	Sample Size (pcs)	σ_{fat} (MPa)	σ_a (MPa)	σ_{max} (MPa)	N (Cycles to failure)			
					Average (\bar{N})	CV	Weibull shape parameter (α)	Weibull scale parameter (β)
WL	8	145.9	84	186.7	1336	0.22	3.26	1350.6
	6	98	65.57	145.7	23862	0.41	2.23	27530
	6	88.4	61.11	135.8	66366	0.21	4.91	72203
	6	78.1	56	124.4	315547	0.35	2.44	400859
VARTM	8	204.3	122.61	272.5	5680	0.20	5.03	6180
	8	152.4	101.79	226.2	27875	0.34	3.01	31378
	9	101	76	168.9	167030	0.31	3.393	186275
	8	85.7	67.01	148.9	2496912	0.19	5.64	2693776

The S-N curves derived from these results (Figure 3) were modeled using a simple power law equation (21) (Eq. 3), with the fitted parameters for both manufacturing processes provided in Table 4.

$$\sigma_{max} = \sigma_0 N_f^{-\frac{1}{K}} \quad \text{Eq. 3}$$

where σ_0 is the initial fatigue strength and K is the slope parameter (Table 5).

Table 5 - The calibrated parameters of S-N diagram for the WL and VARTM manufactured GFRPs.

Manufacturing Process	σ_0 (MPa)	K
WL	314.5	13.3
VARTM	621.7	9.9

The fatigue life of VARTM-manufactured GFRPs demonstrated a significant improvement over WL-manufactured GFRPs, as evident from the S-N curves (Figure 3) and fatigue test results (Table 4). Specifically, at a stress level of 101 MPa, the VARTM samples exhibited a fatigue life of 167030 cycles, whereas WL samples failed after only 66366 cycles. This

corresponds to a 2.5 times greater fatigue life for VARTM composites at this stress level. Furthermore, at a stress level of 85.7 MPa, the VARTM composites exhibited a fatigue life of 2496912 cycles, which is approximately 8 times higher than that of WL samples (315547 cycles at 85.7 MPa). These results align with the calibrated S-N diagram parameters (Table 5), where the initial fatigue strength σ_0 for VARTM composites (621.7 MPa) was nearly double that of WL composites (314.5 MPa). The higher σ_0 and gentler K in VARTM samples illustrate their ability to sustain higher stress levels over more load cycles. This advantage is particularly critical in applications requiring long-term durability, such as wind turbine blades, where cyclic stresses are a major concern.

In terms of the Weibull distribution parameters, α for the WL process ranged from 2.23 to 4.91, indicating moderate variability in fatigue life among the samples. Conversely, the VARTM samples exhibited higher α values, ranging from 3.01 to 5.64, reflecting greater consistency and reliability in their fatigue performance. Additionally, β for VARTM samples was significantly higher across all stress levels, with values substantially exceeding those of the WL samples. This indicates that VARTM composites have a longer service life and preserve their structural integrity more effectively under cyclic loading.

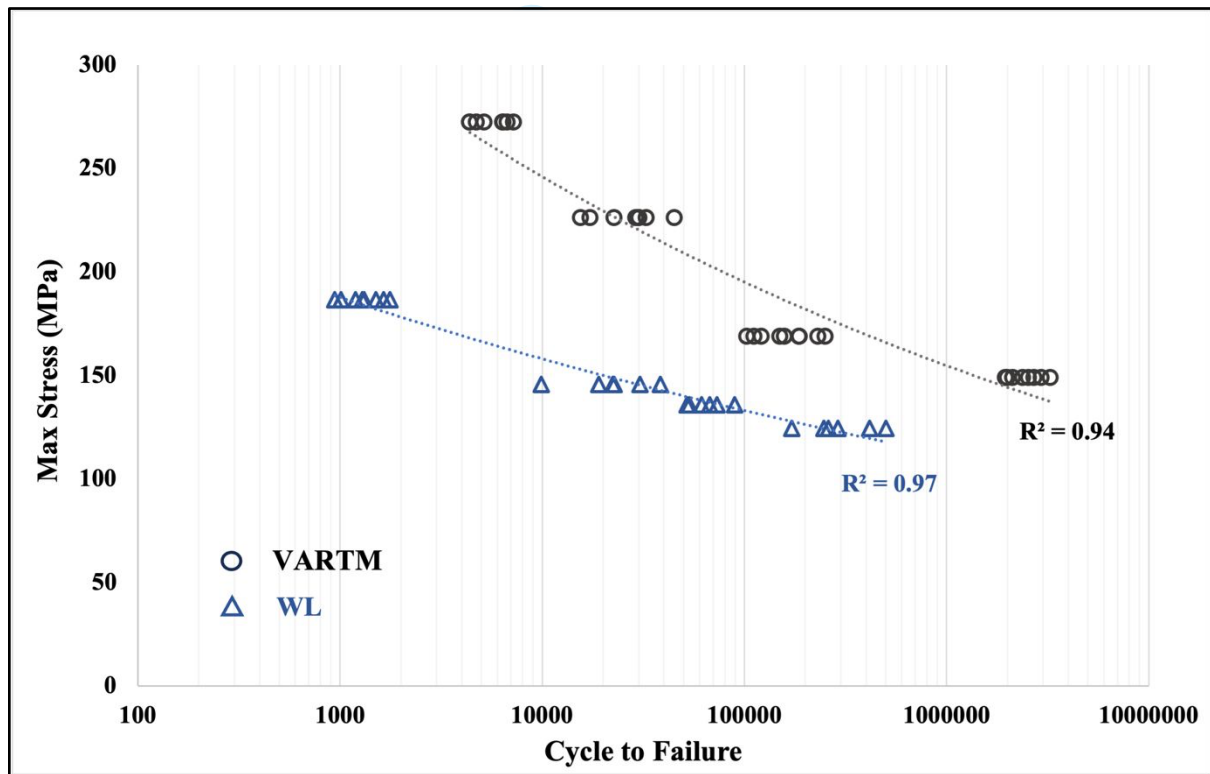


Figure 3- S-N curve of the WL and VARTM manufactured GFRPs at $R = 0.1$ and $f = 8$ Hz

The steeper slope of the VARTM composites S-N curve can be attributed to their higher fiber volume fraction, enhanced fiber/matrix bonding and reduced defect density leading to better fatigue resistance at different stress levels. The S-N curve was fitted using a power-law regression, achieving a goodness-of-fit of $R^2 = 0.98$.

Fatigue failure mechanisms in WL and VARTM samples were studied with SEM quantitatively, focusing on matrix, fiber, and fiber/matrix interfaces. These damage mechanisms were monitored and compared using SEM images of both manufacturing samples (Figure 4), which provide a micro-scale assessment of the fatigued surfaces at 200 μm magnification but not a full macro-scale view of fractured specimens. Delamination was the dominant global failure mechanism in both series, with fiber breakage also apparent. These images allow for an overall assessment of surface morphology, highlighting differences in damage accumulation and failure characteristics between WL and VARTM-manufactured GFRPs. Consistent with Reifsnider's fatigue life stages (16), primary damage mechanisms included matrix cracking, fiber/matrix debonding, fiber pullout, fiber breakage, and delamination. However, the relative dominance of these mechanisms differed significantly between the two manufacturing processes, influencing their fatigue performance.

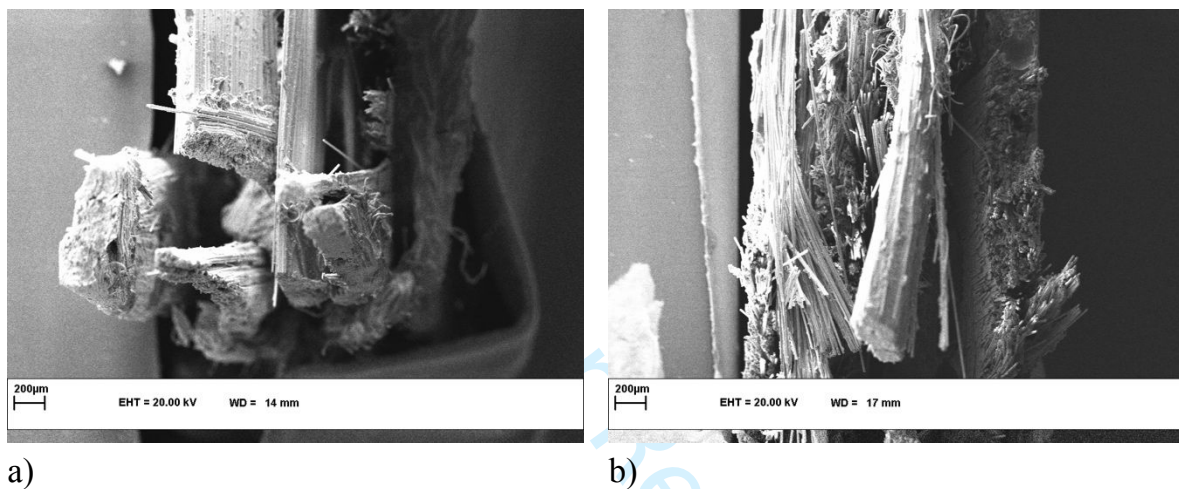


Figure 4– The surface morphology of the fatigued samples a) WL and b) VARTM manufactured GFRPs.

SEM analysis of WL samples displayed manufacturing defects, such as voids, fiber misalignment, and resin-rich zones (Figures 5 and 6). Fiber misalignment was identified by deviations in fiber orientation from the expected stacking sequence, causing non-uniform stress distribution. These imperfections weakened the fiber/matrix interface, leading to inefficient load transfer and increased stress concentrations at defect sites. As a result, fiber pullout was the dominant failure mechanism due to weak interfacial bonding between the fibers and the resin (42). The presence of voids and resin-rich areas further intensified damage progression, accelerating fatigue failure.

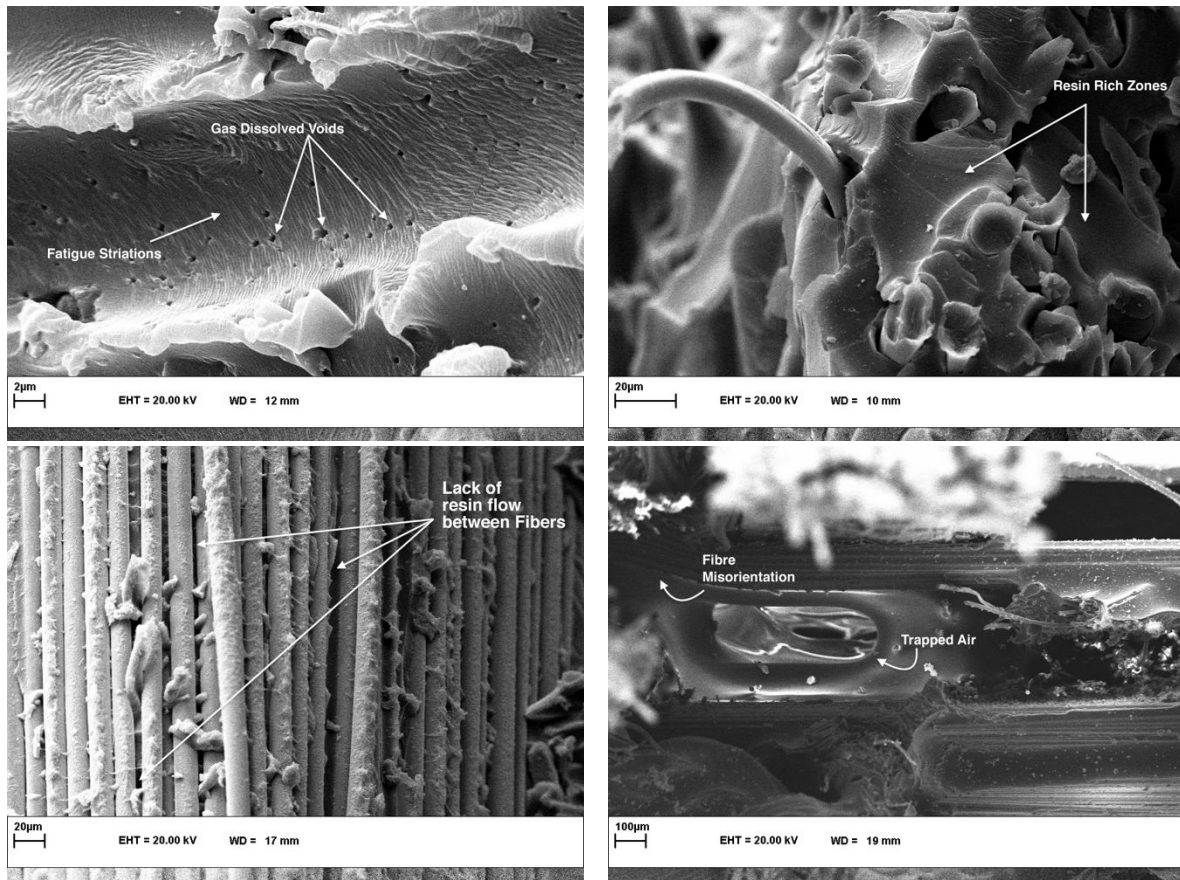


Figure 5- Fiber/matrix interface of the WL fatigued samples at different magnifications

In contrast, VARTM samples exhibited minimal manufacturing defects, resulting in a stronger and more uniform fiber/matrix interface (Figure 7).

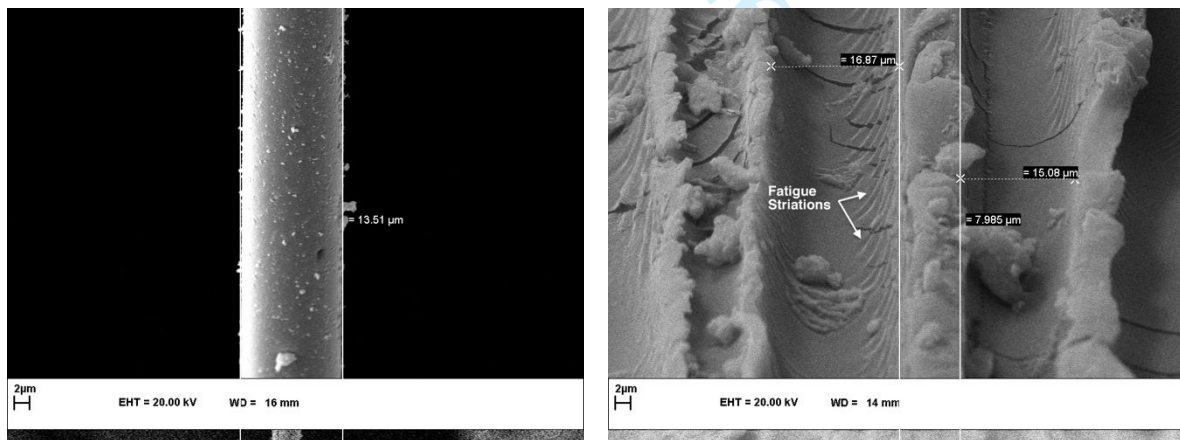


Figure 6- a) Fiber and b) fiber imprints morphology of the WL fatigued samples.

The dominant failure mechanisms in VARTM samples were matrix cracking and fiber breakage, with a reduced amount of fiber pullout compared to WL samples. The presence of matrix residues on the fractured fibers and the bundled form of failed fibers indicate fiber

breakage as the primary failure mechanism. Although both delamination and fiber pullout were observed, they represent distinct failure mechanisms. Delamination refers to interlaminar separation, where plies detach due to weak bonding between adjacent layers, forming a global damage pattern. In contrast, fiber pullout is a localized mechanism where fibers detach individually from the matrix due to weak adhesion at the fiber/matrix interface. WL samples exhibited more fiber pullout, whereas VARTM samples showed a higher incidence of fiber breakage, indicating a stronger fiber/matrix bond. The reduction in fiber pullout was qualitatively checked through SEM image analysis, comparing the number of pulled-out fibers per unit area of the fracture surface, length of exposed fibers, where shorter pullout lengths indicate stronger fiber-matrix bonding and fiber imprints within the matrix, demonstrating whether fibers remained embedded or detached upon failure.

The results confirmed that the VARTM samples had fewer pulled-out fibers, supporting the claim that enhanced fiber-matrix adhesion improved fatigue performance. In addition, the dominant failure mode observed in VARTM samples was cohesive failure, defined as cracking occurring within the matrix material itself. This contrasts with adhesive failure, which occurs at the fiber-matrix interface and was more prevalent in WL samples. The presence of cohesive failure indicates more effective load transfer and improved structural integrity in the VARTM composites. Matrix cracking was also observed as another micro-failure mechanism in the VARTM samples. These observations suggest that failure in VARTM samples is less likely to originate at the fiber-matrix interface (adhesive failure), as seen in WL samples, and is instead dominated by matrix-related mechanisms (cohesive failure). The higher amount of cohesive failure and fewer pulled-out fibers indicate stronger bonding between the fiber and matrix, thereby improving resistance to cyclic loads (43). Also, the absence of striations in fiber imprints further supports the notion that matrix deformation played a lesser role in VARTM composites, reflecting their superior fatigue resistance (Figure 8a).

The fiber weight percentage plays a major role in fatigue life by affecting stiffness, load transfer efficiency, and crack propagation resistance (23). Mortensen et. al (44) has shown that an increase in fiber content leads to improved fatigue life, provided that fiber alignment and interfacial bonding are well maintained. Due to the inherent differences in the manufacturing processes, VARTM samples exhibited a greater fiber weight percentage of about 32% compared to that of WL samples, as excess resin in WL composites is not effectively evacuated during fabrication. This higher fiber weight percentage in VARTM enhances fatigue resistance by improving fiber load distribution and reducing matrix-dominated failure modes. Therefore, while fatigue performance comparisons remain valid, the observed differences should be interpreted considering the influence of fiber weight percentage in addition to other factors such as defect distribution and interface integrity.

It is also important to highlight that the effect of the manufacturing process is more pronounced in fatigue behavior than in tensile properties. As shown in Table 3, the VARTM samples demonstrated a 50.4% higher ultimate tensile strength (UTS) compared to WL samples (374.9 MPa vs. 249.2 MPa). However, the fatigue strength improvement is even more significant. According to the S-N curve parameters in Table 5, the fatigue strength coefficient (σ_0) of the

VARTM samples is nearly 97.6% higher than that of WL samples (621.7 MPa vs. 314.5 MPa), indicating a disproportionately stronger influence of the manufacturing process on fatigue life than on static tensile behavior. This finding emphasizes that fatigue behavior is more sensitive to manufacturing-induced defects, such as voids and poor fiber–matrix bonding, which are effectively reduced in the VARTM process. As such, the fatigue performance advantage of VARTM composites extends well beyond what is observed in monotonic tensile testing alone.

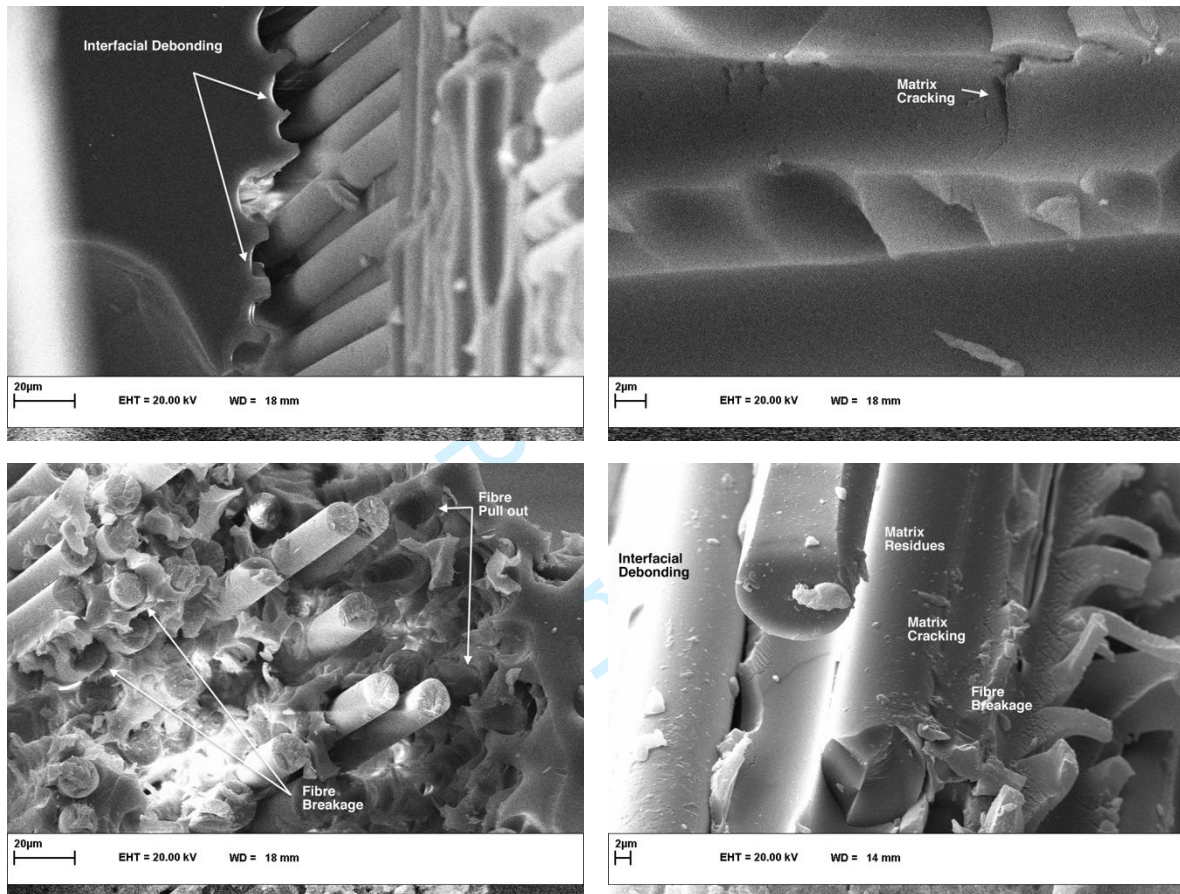
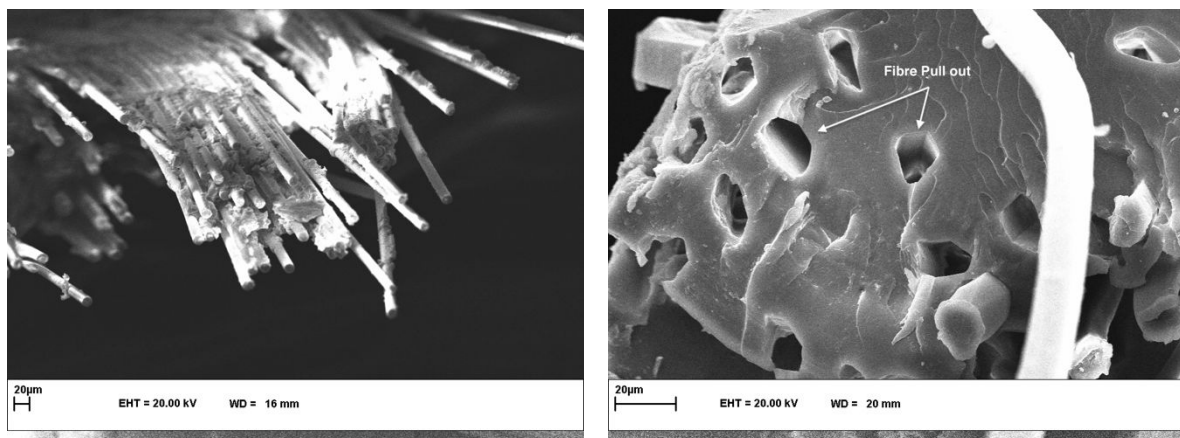


Figure 7- Fiber/matrix interface of the VARTM fatigued samples at different magnifications.



a)

b)

Figure 8- a) Fiber and b) fiber imprints morphology of the VARTM fatigued samples.

The results highlight significant trade-offs between WL and VARTM processes. While WL offers lower initial costs and simpler setup requirements, its process repeatability leads to higher defect rates, resulting in a wider spread of fatigue life data rather than necessarily lowering fatigue performance. However, the increased presence of defects in WL samples leads to premature fatigue failures under high cyclic. In contrast, VARTM, despite requiring greater initial investment due to tooling and vacuum system costs, produces more reliable and longer-lasting components. For industries such as wind turbine manufacturing, where reliability and service time are critical, the long-term advantages of VARTM composite blades outweigh the higher initial costs. A detailed cost-benefit analysis could aid small and medium-scale wind turbine manufacturers in quantifying these trade-offs. The superior fatigue properties of VARTM composites suggest that blade designers can reduce material thickness without compromising durability, leading to lighter and more efficient turbines. Furthermore, the enhanced reliability of VARTM composites decreases the need for conservative safety factors, enabling cost-effective blade designs. A summary of key cost-performance trade-offs between the two manufacturing methods is presented in Table 6 to aid practical decision-making.

Table 6 - Comparison of WL and VARTM methods for GFRP blade manufacturing.

Criteria	WL	VARTM
Initial Equipment Cost	Low	High
Fiber Weight %	52%	69%
Ultimate Tensile Strength	249.2 MPa	374.9 MPa
Ultimate Tensile Strain	2.21 %	2.31 %
Fatigue Strength (σ_0)	314.5 MPa	621.7 MPa
Fatigue Life (at 101 MPa)	66366 Cycles	167030 Cycles
Characteristic Fatigue Life	Lower	Higher
Failure Mode (dominant)	Fiber pullout	Matrix cracking
Manufacturing Defects	Higher	Lower
Process Repeatability	Moderate	High

Conclusion

This study investigated the fatigue behavior of two GFRP laminated composites, each with a repeatable stacking sequence from the root joint of a 100 kW wind turbine blade, fabricated using two different processes: Wet Lay-up (WL) and Vacuum Assisted Resin Transfer Molding (VARTM). The study revealed significant differences between the two manufacturing methods by characterizing the fatigue properties, and physical and mechanical failures. The negative vacuum pressure in the VARTM process led to a marked reduction in manufacturing defects—such as air bubbles, excess resin, dry spots, and fiber misorientation—while also increasing the

1 fiber weight content by 33% compared to WL. These improvements notably enhanced the
2 tensile properties and fiber/matrix interface strength of VARTM composites .

3 The results demonstrated that the average ultimate tensile strength of VARTM samples was
4 50% higher than that of the WL samples, although both exhibited similar ultimate tensile strain.
5 Fatigue testing further highlighted the superior performance of VARTM composites, with a
6 significantly longer fatigue life across all stress levels. For instance, VARTM samples achieved
7 an average fatigue life of 5680 cycles at 204 MPa, compared to just 1336 cycles for WL at 146
8 MPa. Additionally, higher Weibull shape parameters and characteristic life values for VARTM
9 samples indicated greater reliability, while the S-N curve analysis underscored their enhanced
10 durability, with a fatigue strength of 621.7 MPa—nearly double that of WL.

11 Analysis of fatigue fracture surfaces revealed that cohesive failure at the fiber/matrix interface,
12 observed as matrix cracking followed by fiber breakage, was the dominant failure mechanism
13 in VARTM samples. However, fiber pull-out, indicative of lower interfacial strength (adhesive
14 failure), was also noted. Future research should explore the effects of various GFRP composite
15 constituents, including matrix types (polyester and epoxy), stacking sequences, and E-glass
16 fiber treatments like salinization, on the fatigue properties of these composites.

17 These findings provide direct insights for small and medium-sized wind turbine manufacturers,
18 allowing optimized material selection and design to improve blade durability and reduce
19 maintenance costs by switching to the VARTM manufacturing process.

20 **References**

- 21
22 1. Hsiao KT, Heider D. Vacuum assisted resin transfer molding (VARTM) in
23 polymer matrix composites. In *Manufacturing Techniques for Polymer Matrix*
24 *Composites (PMCs)*.: Elsevier; 2012. p. 310-347.
- 25
26 2. Sałasińska K, Cabulis K, Kirpluks P, Kovalov M. The Effect of Manufacture
27 Process on Mechanical Properties and Burning Behavior of Epoxy-Based Hybrid
28 Composites. *Materials (Basel)*. 2022; 15(301): 1-15.
- 29
30 3. Olabi AG, Wilberforce T, Elsaid K, Sayed ET, Salameh T, Abdelkareem MA. A
31 Review on Failure Modes of Wind Turbine Components. *Energies*. 2021 August;
32 14(17): 5241.
- 33
34 4. Hancioglu M, Sozer EM, Advani SG. Comparison of in-plane resin transfer
35 molding and vacuum-assisted resin transfer molding ‘effective’ permeabilities
36 based on mold filling experiments and simulations. *Journal of Reinforced Plastics*
37 *and Composites*. 2019; 39(1-2): 31-44.

5. Zhang C, Liang Z, Wang HP. Vacuum assisted resin transfer molding flow-tracking process and system. Patent No. US007797.075B1. Tallahassee: Florida State University Research Foundation; 2010.
6. Gajjar T, Shah DB, Joshi SJ, Patel KM. Experimental Study of Thickness Gradient and Flow Simulation in VARTM Process. *Fibers and Polymers*. 2020; 21(2): 384-391.
7. Tamakuwala V. Manufacturing of fiber reinforced polymer by using VARTM process: A review. *Materials Today: Proceedings*. 2021; 44(1): 987-993.
8. Lusty AF, Cairns DA, Paquette JA. Alternative damage tolerant materials for wind turbine blades: An overview. Technical. New Mexico: National Technology & Engineering Solutions of Sandia, Sandia National Laboratories; 2021. Report No.: SAND2021-12461.
9. Luo GM, Chen KL, Hsu CT. Acquisition of Key Vacuum-Assisted Resin Transfer Molding Parameters through Reverse Scanning for Application in the Manufacturing of Large Fiber-Reinforced-Plastic Products. *International Journal of Polymer Science*. 2023;: 13.
10. Saad K, Lengyel A. Strengthening Timber Structural Members with CFRP and GFRP: A State-of-the-Art Review. *Polymer*. 2022 June; 14(12): 1-32.
11. Vassilopoulos AP. The history of fiber-reinforced polymer composite laminate fatigue. *International Journal of Fatigue*. 2020;: 1-20.
12. Ganesana C, Joanna P.S. Fatigue Life and Residual Strength prediction of GFRP Composites: An Experimental and Theoretical approach. *Latin American Journal of Solids and Structures*. 2018; 15(7): 1-16.
13. Movahedi-Rad A, Keller T, Vassilopoulos AP. Effect of Loading Pattern on Fatigue Behavior of Laminated Composites. *Proceedings*. 2018; 2: 438-443.
14. Moazzami M, Ayatollahi M, Akhavan-Safar A, Freitas ST, Silva LF. Cyclic aging analysis of CFRP and GFRP composite laminates. *Journal of Composite Materials*. 2023 June; 5(20).
15. Curtis P.T. Tensile fatigue mechanisms in unidirectional polymer matrix composite materials. *International Journal of Fatigue*. 1991; 13(5): 377-382.
16. Reifsnider K, Schulte K, Duke J. Long-Term Fatigue Behavior of Composite Materials O'Brien TK, editor. Philadelphia: American Society for Testing and Materials; 1983.
17. Gaurav A, Singh KK. Fatigue Behavior of FRP Composites and CNT-Embedded FRP Composites: A Review. *Polymer composites*. 2018; 39(6): 1785-1808.

18. Ansari TA, Singh KK, Azam MS. Fatigue damage analysis of fiber-reinforced polymer composites—A review. *Journal of Reinforced Plastics and Composites*. 2018 May; 37(9): 636 - 654.
19. Previtali F, Eyb E. An improved approach for the fatigue calculation of rotor blades based on sector loads. *Wind Engineering*. 2021 January; 45(6).
20. Chrétien A, Tahan A, Pelletier F. Impact of wind turbine nominal power limitation over wind turbine blade remaining useful life and its economic consequences. *Wind Engineering*. 2024 September; 0(0): 1-18.
21. Kim HJ, Cho JR. Numerical Analysis of Fatigue Life of Wind Turbine Blades Reinforced with Graphene Platelets. *Applied Sciences*. 2025; 15(4).
22. Zheng T, Zhao C, He J. Research on fatigue performance of offshore wind turbine blade with basalt fiber bionic plate. *Structures*. 2023; 47: 466-481.
23. Singh AP, Pathak N, Pathak H. Fatigue performance of recycled glass-epoxy composite for wind turbine blades: a multi-scale modeling approach. *Journal of Mechanics and Design*. 2022; 6(2): 19-29.
24. Valizadeh P, Zabet A, Rezaeepazhand J. Investigating the relationship between natural frequency and residual strength and stiffness of cross-ply laminate under cyclic loading. *Polymer International*. 2024;: 1-11.
25. DNVGL-ST-0376. Rotor blades for wind turbines. 2024.
26. ASTM D2734 A. Standard Test Methods for Void Content of Reinforced Plastics. 2023.
27. ASTM D3039/D3039M A. Standard Test Method for Tensile Properties of Polymer Matrix Composite Materials. 2017.
28. Vassilopoulos AP. Fatigue life prediction of composites and composite structures. Second Edition Ltd. E, editor. Cambridge: Woodhead Publishing materials; 2020.
29. Gupta A, Singh M. Investigation of failure behavior of glass fiber reinforced epoxy laminate under fatigue loading. *World Journal of Engineering*. 2025 January; 22(1): 81-88.
30. Sharma N, Singh KK, Ansari MTA. Fatigue life assessment of GFRP composite laminate under axial and transverse fatigue loading. *Materials Today: Proceedings*. 2023.
31. Ferdous W, Manalo A, Peauril J, Salih C, Reddy KR, Yu P, Schubel P, Heyer T. Testing and modelling the fatigue behaviour of GFRP composites – Effect of

stress level, stress concentration and frequency. Engineering Science and Technology, an International Journal. 2020; 23(5): 1223-1232.

32. Nosrati N, Zabett A, Sahebian S. Long-term creep behaviour of E-glass/epoxy composite: Time-temperature superposition principle. *Plastics, Rubber and Composites*. 2020; 49(6): 1-9.
33. Nosrati N, Zabett A, Sahebian S. Stress Dependency of Creep Response for Glass/Epoxy Composite at Nonlinear and Linear Viscoelastic Behavior. 2022 February.
34. ASTM D3479 A. Standard Test Method for Tension-Tension Fatigue of Polymer Matrix Composite Materials. 2023..
35. Dyer KP, Isaac DH. Fatigue behaviour of continuous glass fibre reinforced composites. *Composites Part B: Engineering*. 1998; 29(6): 725-733.
36. Mandell JF, Samborsky DD, Cairns D. *Fatigue of Composite Materials and Substructures for Wind Turbine Blades*. Montana State University; 2002.
37. ASTM E1131 A. Standard Test Method for Compositional Analysis by Thermogravimetry. 2020.
38. Pourhosseini S, Sahebian S, Zabett A. The Effect of Surface Treatment of Glass Fiber on the Mechanical Properties of Epoxy Composite. *Journal of Metallurgical and Materials Engineering*. 2020; 31(2).
39. Bedi R, Chandra R. Fatigue-life distributions and failure probability for glass-fiber reinforced polymeric composites. *Composites Science and Technology*. 2009; 69(9): 1381-1387.
40. Whitney J. "Fatigue Characterization of Composite Materials," in *Fatigue of Fibrous Composite Materials*. 1981.
41. Gao J, An Z, Kou H. Fatigue life prediction of wind turbine rotor blade composites considering the combined effects of stress amplitude and mean stress. *Proceedings of the Institution of Mechanical Engineers, Part O: Journal of Risk and Reliability*. 2018; 232(6): 598-606.
42. Greenhalgh ES. *Failure Analysis and Fractography of Polymer Composites*: Woodhead Publishing; 2009.
43. E Gamstedt EK. Fatigue mechanisms in unidirectional glass-fibre-reinforced polypropylene. *Composites Science and Technology*. 1999; 59: 759-768.
44. Mortensen U.A, Rasmussen S, Mikkelsen L.P, Fraisse A, Andersen T.L. The impact of the fiber volume fraction on the fatigue performance of glass fiber composites. *Composites Part A: Applied Science and Manufacturing*. 2023; 169.